Vol 18 No 2, February 2009
1674-1056/2009/18(02)/0686-13

Chinese Physics B

© 2009 Chin. Phys. Soc.
and IOP Publishing Ltd

Three-dimensional interfacial wave theory of dendritic growth: (II). non-axi-symmetric global wave modes and selection criterion of pattern formation*

Chen Yong-Qiang(陈永强)[a)b)], Tang Xiong-Xin(唐熊忻)[a)c)], and Xu Jian-Jun(徐鉴君)[a)d)†]

[a)] *School of Mathematical Science, Nankai University, Tianjin* 300071, *China*
[b)] *Department of Fundamental Subject, Tianjin Institute of Urban Construction, Tianjin* 300384, *China*
[c)] *School of materials Science and Engineering, University of Science and Technology Beijing, Beijing* 100083, *China*
[d)] *Department of Mathematics and Statistics, McGill University, H3A2K6 Montreal, Canada*

(Received 4 July 2008; revised manuscript received 29 August 2008)

This paper is the continuation of part (I), which completes the derivations of the 3D global wave modes solutions, yields the stability criterion and, on the basis of the results obtained, demonstrates the selection criterion of pattern formation.

Keywords: dendritic growth, pattern formation, interfacial waves, selection criterion

PACC: 6150C, 6870, 6470D, 8130F

1. Introduction

In part (I), we derived the MVE solution up to the first-order approximation.[1] The solution contains a free complex parameter σ_0. In accordance with that, the tip smoothness condition has not been applied yet and the solution involves the simple pole singularity at the points $(\zeta_c, 1)$ and $(0, 1)$ in the extended (ζ, η)-space. The singular point $(\zeta_c, 1)$ is seen in the first-order approximation, but not in the zeroth-order approximation. The presence of the singular point $(\zeta_c, 1)$ plays a vital role in understanding of the selection of dendritic growth and pattern formation, which had been unknown by all previous researchers in the field until its discovery in 1989.[2−4] In part (II) of this work, we shall complete the derivations of 3D global wave modes solutions and further demonstrate the solutions of the fundamental problems: the selection mechanism of dendritic growth and the origin of dendritic pattern formation. The paper is arranged as follows. In Section 2, we explore the properties of the singular point $(\zeta_c, 1)$ and the Stokes phenomenon; in Section 3, we derive the inner solution near the singular point $(\zeta_c, 1)$ in the extended (ζ, η)-space; in Section 4, we derive the inner expansion solution in the singular point $(\zeta_c, 1)$ and apply the tip smoothness condition; in Section 5, we give the quantization conditions of global modes solutions, describe the features of non-axi-symmetrical wave modes, yield the stability criterion and the selection condition of dendritic growth. Finally, in Section 6, we summarize the results and draw the conclusions.

2. Singular point ζ_c of the outer solution and Stokes phenomenon

The location of the singular point $(\zeta_c, 1)$ in the extended (ζ, η)-space depends on the value of σ_0. From

$$F(\zeta_c) = S^2\Big(\frac{\partial \Sigma}{\partial \bar{k}_0}\Big) = 0, \tag{1}$$

combining with the dispersion relationship derived in part (I):

$$\sigma_0 = \Sigma(\zeta, \bar{k}_0) = \frac{\bar{k}_0}{S(\zeta)^2}\left[1 - \frac{2\bar{k}_0^2}{S(\zeta)}\right] - \frac{\mathrm{i}\zeta}{S(\zeta)^2}\bar{k}_0, \tag{2}$$

one finds that

$$\sigma_0 = \sqrt{\frac{2}{27}}\left(\frac{1 - \mathrm{i}\zeta_c}{S}\right)^{3/2}_{\xi=\zeta_c}$$

*Project supported by the Nankai University, China and in part by NSERC Grant of Canada.
†Corresponding author. E-mail: xu@math.mcgill.ca

$$= \mathrm{e}^{-\mathrm{i}3\pi/4}\sqrt{\frac{2}{27}}\left(\frac{\zeta_c+\mathrm{i}}{\zeta_c-\mathrm{i}}\right)^{3/4}, \tag{3}$$

or

$$\sigma_0 = \sqrt{\frac{2}{27}}\left(\frac{r_2}{r_1}\right)^{3/4}\mathrm{e}^{\mathrm{i}3/4(\theta_2-\theta_1-\pi)}, \tag{4}$$

where

$$\zeta_c+\mathrm{i} = r_2\mathrm{e}^{\mathrm{i}\theta_2}; \quad \zeta_c-\mathrm{i} = r_1\mathrm{e}^{\mathrm{i}\theta_1}.$$

From Eq.(3), one can obtain

$$\zeta_c = \zeta(\sigma_0) = \mathrm{i}\left(\frac{|\sigma_0|^{4/3}\mathrm{e}^{\mathrm{i}4\theta/3} - \dfrac{2^{2/3}}{9}}{|\sigma_0|^{4/3}\mathrm{e}^{\mathrm{i}4\theta/3} + \dfrac{2^{2/3}}{9}}\right). \tag{5}$$

The function $\zeta_c = \zeta(\sigma_0)$ is a multiple-valued complex function. One may choose its principal branch, that describes a conformal mapping from complex σ_0 plane to complex plane ζ_c. It is easy to verify that as $\sigma \to 0$, $\zeta_c \to -\mathrm{i}$, as $\sigma_0 \to \infty$, $\zeta_c \to \mathrm{i}$. Finally, as σ_0 on the circle in the σ_0 plane satisfying $|\sigma_0| = \sigma_{\max} = \sqrt{\dfrac{2}{27}}$, ζ_c is on the real axis of ζ_c plane. On the other hand, since we have written σ_0 in the form, $\sigma_0 = \sigma_{0\mathrm{R}} - \mathrm{i}\omega, (\omega > 0)$, we are interested only in the eigenvalue σ_0 belonging to the quarter of the disc: $(|\sigma_0| < \sigma_{\max}, \Re\{\sigma_0\} \geq 0; \Im\{\sigma_0\} < 0)$. In this case, the corresponding range of the function ζ_c is the fourth quadrant of ζ_c plane, namely, $(\Re\{\zeta_c\} > 0, \Im\{\zeta_c\} < 0)$. So, to obtain the physically acceptable continuous solution, one may choose the line in the fourth quadrant that emanates from ζ_c and goes to infinity without passing through the real axis, such as the line (L_1) shown in Fig.1, as the branch cut.

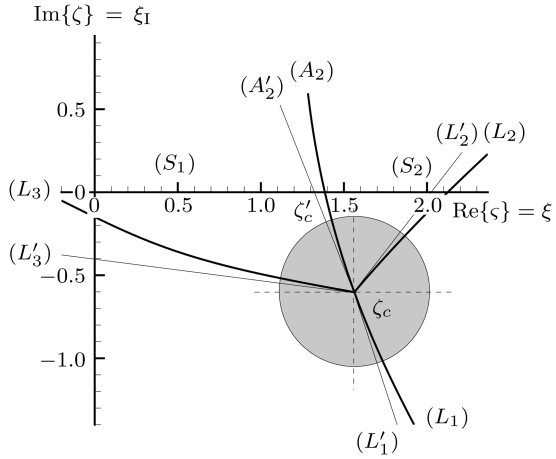


Fig.1. A typical structure of Stokes lines for the system of dendritic growth in the case: $\varepsilon = 0.159$ and $\zeta_c = (1.5627, -0.6017)$, which corresponds to the eigenvalue $\sigma_0 = (1.0841 \times 10^{-5}, -0.2129)$.

From Fig.3 in part (I), it is noted that for fixed $\varepsilon > 0$, as $\xi \gg 1$, we have $\mathrm{Im}\{k_0^{(1)}\} < 0$, while $\mathrm{Im}\{k_0^{(3)}\} > 0$. Hence, as $\xi \to \infty$, the solution H_1 increases exponentially whereas H_3 decreases exponentially. Thus in order to satisfy the root condition in the far field, the following asymptotic form must hold:

$$\tilde{h}_0 \sim D_3' H_3(\xi, \varepsilon) \quad \text{as } \xi \to \infty \ \ (\varepsilon > 0). \tag{6}$$

As a consequence, in the far field one also has

$$\tilde{h}_0 \sim D_3' H_3(\xi, \varepsilon) \quad \text{as } \varepsilon \to 0. \tag{7}$$

This asymptotic condition shows that, in the far-field, the multiple variables asymptotic expansion (MVE) solution obtained in part (I):

$$\tilde{h} \approx D_1\mathrm{e}^{\sigma_0 t_+ + \mathrm{i}\left(\bar{\xi}_+^{(1)} + m\theta\right)} + D_3\mathrm{e}^{\sigma_0 t_+ + \mathrm{i}\left(\bar{\xi}_+^{(3)} + m\theta\right)}, \tag{8}$$

is approximated by a subdominant function $H_3(\zeta, \varepsilon)$. As a consequence, for a fixed $\varepsilon > 0$, the asymptotic form (8) of the solution $\tilde{h}_0$ cannot be applied to the entire complex ζ-plane as a good approximation for the solution $\tilde{h}_0$, due to the so-called Stokes phenomenon.[5]

Let us first use the singular point ζ_c to replace the lower limit of the integral $\xi_1 = 0$ in the definition of ξ_+ and consider the pair of zeroth-order fundamental solutions:

$$H_1(\zeta, \varepsilon) = \exp\left(\frac{\mathrm{i}}{\varepsilon}\int_{\zeta_c}^{\zeta} \bar{k}_0^{(1)}\mathrm{d}\zeta'\right),$$

$$H_3(\zeta, \varepsilon) = \exp\left(\frac{\mathrm{i}}{\varepsilon}\int_{\zeta_c}^{\zeta} \bar{k}_0^{(3)}\mathrm{d}\zeta'\right). \tag{9}$$

Such a pair of fundamental solutions is that used in Eq.(8) multiplied by the reciprocals of the following constant factors

$$\chi_1(\varepsilon) = \frac{1}{\varepsilon}\int_0^{\zeta_c} \bar{k}_0^{(1)}(\zeta')\mathrm{d}\zeta',$$

$$\chi_3(\varepsilon) = \frac{1}{\varepsilon}\int_0^{\zeta_c} \bar{k}_0^{(3)}(\zeta')\mathrm{d}\zeta', \tag{10}$$

respectively. The two fundamental solutions Eq.(9) in the complex ζ-plane are exponential functions of $1/\varepsilon$. As $\varepsilon \to 0$, they are of different orders of magnitude in the complex ζ-plane, except at some isolated lines known as the Stokes lines. The Stokes lines are defined by the integral

$$\Im\left\{\int_{\zeta_c}^{\zeta}\left(\bar{k}_0^{(1)} - k_0^{(3)}\right)\mathrm{d}\zeta'\right\} = 0. \tag{11}$$

On the other hand, the anti-Stokes lines are defined by

$$\Re\Big\{\int_{\zeta_c}^{\zeta}\Big(\bar{k}_0^{(1)}-\bar{k}_0^{(3)}\Big)\mathrm{d}\zeta'\Big\}=0. \tag{12}$$

A sketch of the Stokes lines (L_1), (L_2), (L_3) and anti-Stokes lines (A_1), (A_2), (A_3) of our system are shown in Fig.1. The anti-Stokes line (A_2) divides the entire complex ζ-plane into the sector (S_1) and sector (S_2). The far field $\zeta=\infty$ belongs to sector (S_2), while the tip of the dendrite, $\zeta=0$, belongs to sector (S_1).

Note that when ζ is located on the right side of (L_2), $H_1(\zeta,\varepsilon)\gg H_3(\zeta,\varepsilon)$ exponentially as $\varepsilon\to 0$. As a result, the function $H_1(\zeta,\varepsilon)$ is dominant while the function $H_3(\zeta,\varepsilon)$ is subdominant. When ζ is located on the left side of (L_2), $H_3(\zeta,\varepsilon)\gg H_1(\zeta,\varepsilon)$ exponentially as $\varepsilon\to 0$. In this case, the function $H_3(\zeta,\varepsilon)$ is dominant while the function $H_1(\zeta,\varepsilon)$ is subdominant. Right on the Stokes lines, $H_1(\zeta,\varepsilon)=O\big(H_3(\zeta,\varepsilon)\big)$, the two functions have the same order of magnitudes as $\varepsilon\to 0$. When ζ moves across the Stokes line, the former subdominant of these two functions becomes dominant.

According to the turning point theory, the pair of coefficients of the solution (8) will be different in different sectors (S_1) and (S_2). Let us denote the coefficients of the solution (8) in (S_2) by $\{D_1', D_3'\}$ and by $\{D_1, D_3\}$ in (S_1). From the far field condition, we derive $D_1'=0$, and we also have $D_3=D_3'$. The connection condition between the coefficients $\{D_1, D_3=D_3'\}$ in sector (S_1) and $\{D_1'=0, D_3'\}$ in sector (S_2) is to be derived by matching the outer solution (8) with the inner solution near the singular point ζ_c.

3. The inner solutions near the singular point ζ_c

In the previous section, we find that the MVE solution fails to be valid at the point $(\zeta_c,1)$ in the extended (ζ,η)-space. This implies that the solutions in the vicinity of the point $(\zeta_c,1)$ in the (ζ,η)-space: $|\zeta-\zeta_c|\ll 1$; $|\eta-1|\ll 1$, no longer have a multiple scale structure. Thus, to derive the inner asymptotic form of solutions we must start with the perturbed system (24)–(30) given in part (I)[1] and construct a different asymptotic expansion. For this purpose, we introduce the inner variables

$$\zeta_*=\frac{\zeta-\zeta_c}{\varepsilon^{\alpha}},$$

$$\eta_*=\frac{\eta-1}{\varepsilon^{\alpha}}, \tag{13}$$

where α is to be determined later. With the inner variables, the interface shape function is

$$\eta_{\mathrm{s}}(\zeta,\theta,t)=1+\frac{\tilde{h}}{\eta_0^2}=1+\varepsilon^{\alpha}\eta_{*\mathrm{s}}. \tag{14}$$

For

$$\eta_{*\mathrm{s}}=\frac{\hat{h}(\zeta_*,\theta,t)}{\eta_0^2}, \tag{15}$$

we have

$$\tilde{h}(\zeta,\theta,t)=\varepsilon^{\alpha}\hat{h}(\zeta_*,\theta,t). \tag{16}$$

Accordingly, we put

$$\tilde{T}(\zeta,\eta,\theta,t)=\varepsilon^{\alpha}\hat{T}(\zeta_*,\eta_*,\theta,t);\quad \tilde{T}_{\mathrm{S}}(\zeta,\eta,\theta,t)=\varepsilon^{\alpha}\hat{T}_{\mathrm{S}}(\zeta_*,\eta_*,\theta,t). \tag{17}$$

We seek the mode solutions and make the inner expansions

$$\hat{T}(\zeta_*,\eta_*,\theta,t)=\Big[\hat{\nu}_0(\varepsilon)\hat{T}_0(\zeta_*,\eta_*)+\nu_1(\varepsilon)\hat{T}_1(\zeta_*,\eta_*)+\dots\Big]\mathrm{e}^{\sigma t/\varepsilon\eta_0^2+\mathrm{i}m\theta},$$

$$\hat{T}_{\mathrm{S}}(\zeta_*,\eta_*,\theta,t)=\Big[\hat{\nu}_0(\varepsilon)\hat{T}_{\mathrm{S}0}(\zeta_*,\eta_*)+\nu_1(\varepsilon)\hat{T}_{\mathrm{S}1}(\zeta_*,\eta_*)+\dots\Big]\mathrm{e}^{\sigma t/\varepsilon\eta_0^2+\mathrm{i}m\theta},$$

$$\hat{h}(\zeta_*,\theta,t)=\Big[\hat{\nu}_0(\varepsilon)\hat{h}_0(\zeta_*)+\nu_1(\varepsilon)\hat{h}_1(\zeta_*)+\dots\Big]\mathrm{e}^{\sigma t/\varepsilon\eta_0^2+\mathrm{i}m\theta}. \tag{18}$$

To find the inner solution, we need further to apply the transformation first introduced in Ref.[2] and transform the solution $\tilde{h}_0(\zeta)$ into a new unknown function $W_0(\zeta)$,

$$\tilde{h}_0(\zeta)=W_0(\zeta)\exp\Big[\frac{\mathrm{i}}{\varepsilon}\int_{\zeta_c}^{\zeta}k_c(\xi_1)\ \mathrm{d}\xi_1\Big], \tag{19}$$

where the reference wave number function $k_c(\zeta)$ is to be chosen later. It will be seen that

$$\mathrm{Re}\{k_0^{(3)}\} < \mathrm{Re}\{k_c\} < \mathrm{Re}\{k_0^{(1)}\}\,. \tag{20}$$

In the outer region we have

$$H_1 = W_0^{(+)}(\zeta)\exp\left[\frac{\mathrm{i}}{\varepsilon}\int_{\zeta_c}^{\zeta_*} k_c(\xi_1)\ \mathrm{d}\xi_1\right] \tag{21}$$

and

$$H_3 = W_0^{(-)}(\zeta)\exp\left[\frac{\mathrm{i}}{\varepsilon}\int_{\zeta_c}^{\zeta_*} k_c(\xi_1)\ \mathrm{d}\xi_1\right]. \tag{22}$$

The general outer solutions for W_0 may be written in the form

$$W_0 = D_1 W_0^{(+)} + D_3 W_0^{(-)}\ . \tag{23}$$

Then the wave number function for the $W_0^{(+)}$ wave is $k_0^{(+)} = k_0^{(1)} = k_0^{(1)} - k_c$. Since $\mathrm{Re}\{k_0^{(+)}\} > 0$, the phase velocity of the $W_0^{(+)}$ wave is positive and, as such, it is an outgoing wave. On the other hand, the wave number function for the $W^{(-)}$ wave is $k_0^{(-)} = k_0^{(3)} = k_0^{(3)} - k_c$, and $\mathrm{Re}\{k_0^{(-)}\} < 0$. Hence, the $W_0^{(-)}$ wave is an incoming wave with a negative phase velocity. One can draw the following diagram of the relation between the H waves and the W waves:

H_1 wave $\iff$ $W^{(+)}$
(short-wave branch) (outgoing wave);

H_3 wave $\iff$ $W^{(-)}$
(long-wave branch) (incoming wave).

In accordance with the above, in the inner region we can set

$$\hat{h}_0(\zeta_*) = \hat{W}_0(\zeta_*)\exp\left\{\frac{\mathrm{i}}{\varepsilon}\int_{\zeta_c}^{\zeta} k_c(\xi_1)\ \mathrm{d}\xi_1\right\}. \tag{24}$$

We also set

$$k_c(\zeta) = \mathrm{e}^{-\mathrm{i}\pi/4}\sqrt{\frac{S}{6}\ (\zeta+\mathrm{i})} \quad \left(\ \mathrm{Re}\{k_c\} > 0\right) \tag{25}$$

and

$$\alpha = \frac{2}{3}, \quad \zeta_* = \frac{(\zeta-\zeta_c)}{\varepsilon^{2/3}}, \tag{26}$$

then the leading-order approximation of the inner equation is found to be the Airy equation[5,6]

$$\frac{\mathrm{d}^2\hat{W}_0}{\mathrm{d}\zeta_*^2}\ +\ A^2\zeta_*\hat{W}_0\ = 0\,, \tag{27}$$

where

$$A = \left(\frac{S^3}{6k_c}\frac{\partial\Sigma_c}{\partial\zeta}\right)^{1/2}_{\zeta=\zeta_c} = \mathrm{i}\sqrt{\frac{1}{6}}\left(\frac{\zeta_c+\mathrm{i}}{\zeta_c-\mathrm{i}}\right)^{1/4}$$

$$\left(\frac{\pi}{2} < \arg\{A\} < \frac{3\pi}{4}\right). \tag{28}$$

This can be written as the standard Airy equation

$$\frac{\mathrm{d}^2\hat{W}_0}{\mathrm{d}\hat{\zeta}_*^2}\ +\hat{\zeta}_*\hat{W}_0\ = 0, \tag{29}$$

by introducing the new inner variable

$$\hat{\zeta}_* = \frac{A^{2/3}}{\varepsilon^{2/3}}(\zeta-\zeta_c). \tag{30}$$

The general solution of the above Airy equation is

$$\hat{W}_0 = D_{*1}\hat{\zeta}_*^{1/2}\mathrm{H}^{(1)}_{1/3}(\zeta) + D_{*2}\hat{\zeta}_*^{1/2}\mathrm{H}^{(2)}_{1/3}(\zeta), \tag{31}$$

$$\left(\zeta = \frac{2}{3}\hat{\zeta}_*^{3/2}\right),$$

where $\mathrm{H}^{(1)}_\nu(z)$ is ν^{th}-order Hankel function of the first kind, while $\mathrm{H}^{(2)}_\nu(z)$ is the Hankel function of the second kind. In order to match with the outer solution, which satisfies the downstream far-field condition (7) as $\hat{\zeta}_* \to \infty$, the inner solution must be

$$\hat{W}_0 = D_*\hat{\zeta}_*^{1/2}\mathrm{H}^{(2)}_{1/3}(\zeta). \tag{32}$$

By matching the inner solution with the outer solution in the sectors (S_1) and (S_2), we verify

$$k_1 \sim \frac{\mathrm{i}}{4(\zeta-\zeta_c)} + o(1), \quad R_1(\zeta_c) = 0, \tag{33}$$

and obtain the connection condition

$$\frac{D_1}{D_3} = \mathrm{e}^{\mathrm{i}\pi/2}, \quad D_3 = D_3'. \tag{34}$$

4. Tip inner solution in the tip region

As indicated in the previous section, the MVE solution is also invalid in the vicinity of the point $(\zeta = 0, \eta = 1)$ in the (ζ, η)-space, which may be called the tip region. So, one needs to find the new asymptotic form of solution in this region. In doing so, we define the tip inner variables

$$\hat{\xi} = \frac{\hat{k}\xi}{\varepsilon}, \quad \hat{\zeta} = \frac{\hat{k}\zeta}{\varepsilon},$$

$$\hat{\eta} = \frac{(\eta-1)}{\varepsilon}, \quad \hat{t} = \frac{t}{\eta_0^2\varepsilon}, \tag{35}$$

where $|\zeta| \ll \varepsilon$, and $|\eta - 1| \ll 1$. The tip solution can be expressed as a function of these inner variables and expanded in the following asymptotic form as $\varepsilon \to 0$:

$$\hat{T}(\hat{\xi},\hat{\eta},\theta,\hat{t}) = \Big\{\hat{\mu}_0(\varepsilon)\hat{T}_0 + \hat{\mu}_1(\varepsilon)\hat{T}_1 + \dots\Big\}\mathrm{e}^{\mathrm{i}m\theta+\sigma\hat{t}},$$

$$\hat{T}_{\mathrm{S}}(\hat{\xi},\hat{\eta},\theta,\hat{t}) = \Big\{\hat{\mu}_0(\varepsilon)\hat{T}_{\mathrm{S}0} + \hat{\mu}_1(\varepsilon)\hat{T}_{\mathrm{S}1} + \dots\Big\}\mathrm{e}^{\mathrm{i}m\theta+\sigma\hat{t}},$$

$$\hat{h}(\hat{\xi},\theta,\hat{t}) = \Big\{\hat{\mu}_0(\varepsilon)\hat{h}_0 + \hat{\mu}_1(\varepsilon)\hat{h}_1 + \dots\Big\}\mathrm{e}^{\mathrm{i}m\theta+\sigma\hat{t}},$$

$$\hat{k} = \hat{k}_0 + \varepsilon\hat{k}_1 + \dots. \tag{36}$$

At the zeroth-order approximation in the tip region, the system (24)–(30) given in part (I)[1] can be reduced to

$$\hat{k}_0^2\frac{\partial^2\hat{T}_0}{\partial\hat{\xi}^2} + \frac{\partial^2\hat{T}_0}{\partial\hat{\eta}^2} + \frac{\hat{k}_0^2}{\hat{\xi}}\frac{\partial\hat{T}_0}{\partial\hat{\xi}} - \frac{m^2\hat{k}_0^2}{\hat{\xi}^2}\hat{T}_0 = 0,$$

$$\hat{k}_0^2\frac{\partial^2\hat{T}_{\mathrm{S}0}}{\partial\hat{\xi}^2} + \frac{\partial^2\hat{T}_{\mathrm{S}0}}{\partial\hat{\eta}^2} + \frac{\hat{k}_0^2}{\hat{\xi}}\frac{\partial\hat{T}_{\mathrm{S}0}}{\partial\hat{\xi}} - \frac{m^2\hat{k}_0^2}{\hat{\xi}^2}\hat{T}_{\mathrm{S}0} = 0 \tag{37}$$

with the boundary conditions at $\hat{\eta}=0$

$$\hat{T}_0 = \hat{T}_{\mathrm{S}0} + \hat{h}_0, \tag{38}$$

$$\hat{T}_{\mathrm{S}0} = \hat{k}_0^2\Big(\frac{\partial^2\hat{h}_0}{\partial\hat{\xi}^2} + \frac{1}{\hat{\xi}}\frac{\partial\hat{h}_0}{\partial\hat{\xi}} - \frac{m^2}{\hat{\xi}^2}\hat{h}_0\Big), \tag{39}$$

$$\frac{\partial}{\partial\hat{\eta}}\big(\hat{T}_0 - \hat{T}_{\mathrm{S}0}\big) + \sigma_0\hat{h}_0 = 0. \tag{40}$$

This system admits the inner solutions

$$\hat{T}_0 = \hat{a}_0\mathrm{H}_m^{(1)}(\hat{\xi})\mathrm{e}^{-\hat{k}_0\hat{\eta}},$$

$$\hat{T}_{\mathrm{S}0} = \hat{a}_{S0}\mathrm{H}_m^{(1)}(\hat{\xi})\mathrm{e}^{\hat{k}_0\hat{\eta}},$$

$$\hat{h}_0 = \hat{d}_0\mathrm{H}_m^{(1)}(\hat{\xi}), \tag{41}$$

where $\mathrm{H}_m^{(1)}(\hat{\xi})$ is the m-order Hankel function of the first kind.

From the boundary conditions (38)–(40), one obtains

$$\hat{a}_0 = (1-\hat{k}_0^2)\hat{d}_0\,, \quad \hat{a}_{S0} = -\hat{k}_0^2\hat{d}_0, \tag{42}$$

and the local dispersion relation in the tip region

$$\sigma_0 = \hat{k}_0\big(1-2\hat{k}_0^2\big). \tag{43}$$

For fixed σ_0, Eq.(43) has three roots for $\hat{k}_0$. Comparing the local dispersion relation in the tip region (43) with the local dispersion relation in the outer region (2), one can evidently write

$$\hat{k}_0^{(1)} = \bar{k}_0^{(1)}(0),$$

$$\hat{k}_0^{(2)} = \bar{k}_0^{(2)}(0),$$

$$\hat{k}_0^{(3)} = \bar{k}_0^{(3)}(0). \tag{44}$$

The root $\hat{k}_0^{(2)}$ must be ruled out due to the fact that $\mathrm{Re}\big\{\hat{k}_0^{(2)}\big\} < 0$. Therefore, the general solution of $\hat{h}_0$ in the tip region is

$$\hat{h}_0 = \hat{d}_0^{(1)}\mathrm{H}_m^{(1)}\Big(\frac{\hat{k}_0^{(1)}\xi}{\varepsilon}\Big) + \hat{d}_0^{(3)}\mathrm{H}_m^{(1)}\Big(\frac{\hat{k}_0^{(3)}\xi}{\varepsilon}\Big). \tag{45}$$

The above tip inner solution must match with the outer solution. By setting

$$\hat{d}_0^{(1)} = d_0, \quad \hat{d}_0^{(3)} = -\hat{Q}_0 d_0, \tag{46}$$

we can express the tip inner solution as

$$\hat{h}_0 = d_0\left\{H_{\mathrm{m}}^{(1)}\Big(\frac{\hat{k}_0^{(1)}\xi}{\varepsilon}\Big) - \hat{Q}_0\mathrm{H}_m^{(1)}\Big(\frac{\hat{k}_0^{(3)}\xi}{\varepsilon}\Big)\right\}. \tag{47}$$

As $\hat{\xi}\to\infty$, one has

$$\hat{h}_0 \approx d_0\sqrt{\frac{2}{\pi}}\mathrm{e}^{-(m+\frac{1}{2})\frac{\pi}{2}}\left\{\sqrt{\frac{\varepsilon}{k_0^{(1)}(0)\xi}}\,\mathrm{e}^{\frac{\mathrm{i}k_0^{(1)}(0)\xi}{\varepsilon}} - \hat{Q}_0\sqrt{\frac{\varepsilon}{k_0^{(3)}(0)\xi}}\,\mathrm{e}^{\frac{\mathrm{i}k_0^{(3)}(0)\xi}{\varepsilon}}\right\}. \tag{48}$$

Now we need to match the tip inner solution (47) with the outer solution derived in the last section, namely,

$$\hat{\mu}_0(\varepsilon)\sqrt{\frac{2\varepsilon}{\pi}}d_0\left\{\sqrt{\frac{1}{\hat{k}_0^{(1)}\hat{\xi}}}\mathrm{e}^{\frac{\mathrm{i}\hat{k}_0^{(1)}\xi}{\varepsilon}}-\hat{Q}_0\sqrt{\frac{1}{\hat{k}_0^{(3)}\hat{\xi}}}\mathrm{e}^{\frac{\mathrm{i}\hat{k}_0^{(3)}\xi}{\varepsilon}}\right\}$$

$$\Updownarrow$$

$$\tilde{\mu}_0(\varepsilon)\left(D_1\exp\left\{\frac{\mathrm{i}}{\varepsilon}\int_{\zeta_c}^{\xi}\bar{k}_0^{(1)}\mathrm{d}\xi'\right\}+D_3\exp\left\{\frac{\mathrm{i}}{\varepsilon}\int_{\zeta_c}^{\xi}\bar{k}_0^{(3)}\mathrm{d}\xi'\right\}\right)$$
$$=\tilde{\mu}_0(\varepsilon)\left[D_1\mathrm{e}^{-\mathrm{i}\chi_1}\exp\left\{\frac{\mathrm{i}}{\varepsilon}\int_0^{\xi}\bar{k}_0^{(1)}\mathrm{d}\xi'\right\}+D_3\mathrm{e}^{-\mathrm{i}\chi_3}\exp\left\{\frac{\mathrm{i}}{\varepsilon}\int_0^{\xi}\bar{k}_0^{(3)}\mathrm{d}\xi'\right\}\right].$$

Hereby, we have used the previously defined notations (10):

$$\chi_1(\varepsilon)=\frac{1}{\varepsilon}\int_0^{\zeta_c}\bar{k}_0^{(1)}(\xi')\mathrm{d}\xi',$$
$$\chi_3(\varepsilon)=\frac{1}{\varepsilon}\int_0^{\zeta_c}\bar{k}_0^{(3)}(\xi')\mathrm{d}\xi'.$$

In order to satisfy the above matching condition, the parameter σ_0 must be a proper function of ε, such that as $\varepsilon\to 0$, the two functions, $\exp\left\{-\mathrm{i}\chi_1+\frac{\mathrm{i}}{\varepsilon}\int_0^{\xi}\bar{k}_0^{(1)}\mathrm{d}\xi'\right\}$ and $\exp\left\{-\mathrm{i}\chi_3+\frac{\mathrm{i}}{\varepsilon}\int_0^{\xi}\bar{k}_0^{(3)}\mathrm{d}\xi'\right\}$ are of the same order of magnitude. Therefore, the origin $\zeta=0$ will not on a Stokes line, unless $\left|\bar{k}_0^{(1)}(0)\right|=\left|\bar{k}_0^{(3)}(0)\right|$.

Thus it follows from the matching condition that

$$\hat{\mu}_0(\varepsilon)\varepsilon^{1/2}=\tilde{\mu}_0(\varepsilon), \tag{49}$$

and

$$\frac{D_3\mathrm{e}^{-\mathrm{i}\chi_3}}{D_1\mathrm{e}^{-\mathrm{i}\chi_1}}=-\mathrm{i}\mathrm{e}^{\mathrm{i}(\chi_1-\chi_3)}=-\hat{Q}_0\left(\frac{\bar{k}_0^{(1)}(0)}{\bar{k}_0^{(3)}(0)}\right)^{1/2}, \tag{50}$$

or,

$$\hat{Q}_0=\hat{Q}_0(\sigma_0,\varepsilon)=\mathrm{i}\mathrm{e}^{\mathrm{i}(\chi_1-\chi_3)}\left(\frac{\bar{k}_0^{(3)}(0)}{\bar{k}_0^{(1)}(0)}\right)^{1/2}. \tag{51}$$

Up to this point, the first-order asymptotic solution contains a free parameter, σ_0.

5. Global trapped-wave (GTW) modes and the quantization condition

We now turn to the second step: constructing the global eigen-modes and deriving the quantization condition for the eigenvalues by applying the tip smoothness condition

$$\frac{\partial}{\partial\hat{\xi}}\{\hat{T},\hat{T}_{\mathrm{S}},\hat{h}\}=0 \tag{52}$$

to the asymptotic solutions obtained above. Note that as $\hat{\xi}\to 0$,

$$\mathrm{H}_m^{(1)}\left(\frac{\hat{k}_0\xi}{\varepsilon}\right)\sim\begin{cases}-\mathrm{i}\dfrac{(m-1)!}{\pi}\left(\dfrac{2\varepsilon}{\hat{k}_0\xi}\right)^m+O\left(\dfrac{\hat{k}_0\xi}{2\varepsilon}\right)^m, & (m>0),\\ \mathrm{i}\dfrac{2}{\pi}\ln\left(\dfrac{\hat{k}_0\xi}{\varepsilon}\right)+1+\mathrm{i}\dfrac{2}{\pi}(\gamma-\ln 2)+O\left(\dfrac{\hat{k}_0\xi}{\varepsilon}\right), & (m=0),\end{cases}$$

(see p360 in Ref.[6]).

To examine the tip smoothness condition $\hat{h}_0(0)=O(1),\hat{h}_0'(0)=0$, one needs to investigate the behaviour of the function $\hat{h}_0(\hat{\xi})$ as $\hat{\xi}\to 0$ for each of the cases $m=0,1,2,\ldots$, respectively.

- For the case $m=0$, we have

$$\hat{h}_0(\xi)\approx d_0\left\{\mathrm{i}\frac{2}{\pi}\ln\left(\frac{\hat{k}_0^{(1)}\xi}{\varepsilon}\right)-\mathrm{i}\hat{Q}_0\frac{2}{\pi}\ln\left(\frac{\hat{k}_0^{(3)}\xi}{\varepsilon}\right)\right\}+O(1).$$

To ensure $\hat{h}_0(0) = O(1)$, one must set $\hat{Q}_0 = 1$. Meanwhile, the tip smoothness condition is satisfied, since

$$\hat{h}_0'(0) = 0.$$

- For the case $m = 1$, we have

$$\hat{h}_0(\hat{\xi}) \approx d_0 \left\{ \Big(\frac{\hat{k}_0^{(1)}\xi}{2\varepsilon} - \mathrm{i}\frac{2\varepsilon}{\pi \hat{k}_0^{(1)}\xi} \Big) - \hat{Q}_0 \Big(\frac{\hat{k}_0^{(3)}\xi}{2\varepsilon} - \mathrm{i}\frac{2\varepsilon}{\pi \hat{k}_0^{(3)}\xi} \Big) \right\}.$$

To ensure $\hat{h}_0(0) = O(1)$, one must set $\hat{Q}_0 = \dfrac{\hat{k}_0^{(3)}}{\hat{k}_0^{(1)}}$. However, in the meantime, one has

$$\hat{h}_0'(0) = \frac{d_0 \hat{k}_0^{(3)}}{2} \left\{ \frac{\hat{k}_0^{(1)}}{\hat{k}_0^{(3)}} - \frac{\hat{k}_0^{(3)}}{\hat{k}_0^{(1)}} \right\} \neq 0.$$

It is seen that the tip smoothness condition cannot be satisfied, as $\hat{k}_0^{(1)} \neq \hat{k}_0^{(3)}$.

- For the case $m > 1$, we have

$$\hat{h}_0(\hat{\xi}) \approx d_0 \left\{ \left[\frac{1}{m!} \Big(\frac{\hat{k}_0^{(1)}\xi}{2\varepsilon} \Big)^m - \mathrm{i}\frac{(m-1)!}{\pi} \Big(\frac{2\varepsilon}{\hat{k}_0^{(1)}\xi} \Big)^m \right] - \hat{Q}_0 \left[\frac{1}{m!} \Big(\frac{\hat{k}_0^{(3)}\xi}{2\varepsilon} \Big)^m - \mathrm{i}\frac{(m-1)!}{\pi} \Big(\frac{2\varepsilon}{\hat{k}_0^{(3)}\xi} \Big)^m \right] \right\}.$$

To ensure $\hat{h}_0(0) = O(1)$, one must set $\hat{Q}_0 = \left(\dfrac{\hat{k}_0^{(3)}}{\hat{k}_0^{(1)}} \right)^m$. In the meantime, one has

$$\hat{h}_0'(0) = 0,$$

hence the tip smoothness condition is satisfied.

In summary, in order for tip solution (47) to satisfy the tip condition, one must set

$$\hat{Q}_0 = \left(\frac{\hat{k}_0^{(3)}}{\hat{k}_0^{(1)}} \right)^m = \left(\frac{\bar{k}_0^{(3)}(0)}{\bar{k}_0^{(1)}(0)} \right)^m, \tag{53}$$

and the modes $m = 0$ and $m = 2, 3, \ldots$ are allowable. The $m = 0$ mode gives an axi-symmetric interfacial travelling wave, while $m = 2, 3, \ldots$ modes give multi-arms spiral interfacial wave.

Formula (53) is the quantization condition for the eigenvalues. Combining with Eq.(51), one may rewrite Eq.(53) in the form

$$\begin{aligned} &\frac{1}{\varepsilon} \int_0^{\zeta_c} \Big(\bar{k}_0^{(1)} - \bar{k}_0^{(3)} \Big) \mathrm{d}\zeta \\ &= \left(2n + 1 + \frac{1}{2} - \frac{2m-1}{2}\theta_0 \right) \pi \\ &\quad + \mathrm{i}\,\frac{2m-1}{2} \ln \alpha_0 \\ &\quad (m = 0, 2, 3, \ldots; \quad n = 0, 1, 2, \ldots), \end{aligned} \tag{54}$$

where

$$\alpha_0 \, \mathrm{e}^{\mathrm{i}\theta_0 \pi} = \frac{\bar{k}_0^{(1)}(0)}{\bar{k}_0^{(3)}(0)} \, . \tag{55}$$

This quantization condition gives a discrete set of complex eigenvalues

$$\sigma_0^{(m,n)} \quad (m = 0, 2, 3, \ldots; \quad n = 0, 1, 2, \ldots)$$

as functions of the parameters ε. For the special axi-symmetric case ($m = 0$), we have

$$\begin{aligned} &\frac{1}{\varepsilon} \int_0^{\zeta_c} \Big(\bar{k}_0^{(1)} - \bar{k}_0^{(3)} \Big) \mathrm{d}\zeta \\ &= \left(2n + 1 + \frac{1}{2} + \frac{1}{2}\theta_0 \right) \pi - \mathrm{i}\, \frac{1}{2} \ln \alpha_0. \end{aligned} \tag{56}$$

This quantization condition gives a discrete set of complex eigenvalues

$$\sigma_0^{(0,n)} \quad (n = 0, 1, 2, \ldots).$$

Here, it should be emphasized that as a necessary condition, for a physically acceptable mode, the location of the singular point ζ_c must be in the fourth quadrant, satisfying $\Re\{\zeta_c\} > 0$ and $\Im\{\zeta_c\} < 0$.

We find that the system allows the following (m, n) global eigen-modes:

- The axi-symmetric modes:

$$(0, 0), (0, 1), (0, 2), (0, 3), \ldots;$$

- The multi-arms spiral modes:

$$(2, 1), (2, 2); (3, 2), (3, 3); (4, 2), (4, 3), (4, 4); \ldots$$

In the zeroth-order approximation, the variations of the real part and imaginary part of eigenvalues, σ_0 and ω_0 with ε, are shown in Figs.2 and 3, respectively. The distribution of the eigenvalues σ_0 with different ε is shown in Fig.4. Our numerical results show that

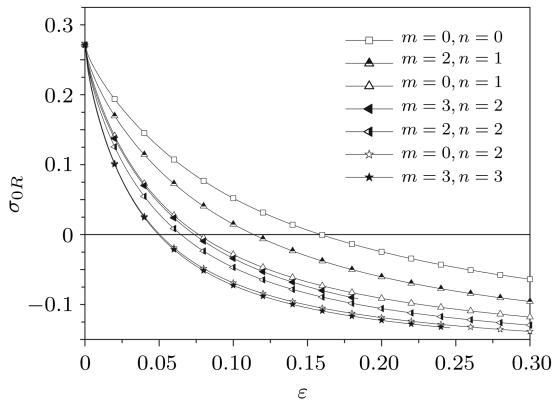


Fig.2. The variations of the real part of the zeroth-order approximation of eigenvalues, $\sigma_{0\mathrm{R}}$ with ε of the modes $(0,0)$,$(0,1)$,$(0,2)$; $(2,1)$, $(2,2)$; $(3,2)$, $(3,3)$ for the case $\eta_0^2 = 0.01$.

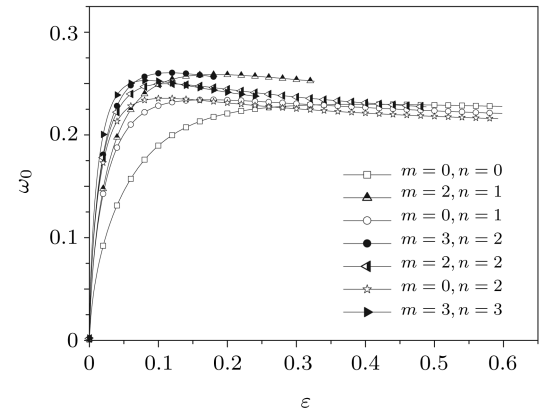


Fig.3. The variations of the imaginary part of the zeroth-order approximation of eigenvalues, ω_0 with ε, of the modes $(0,0)$,$(0,1)$,$(0,2)$; $(2,1)$, $(2,2)$; $(3,2)$, $(3,3)$ for the case $\eta_0^2 = 0.01$.

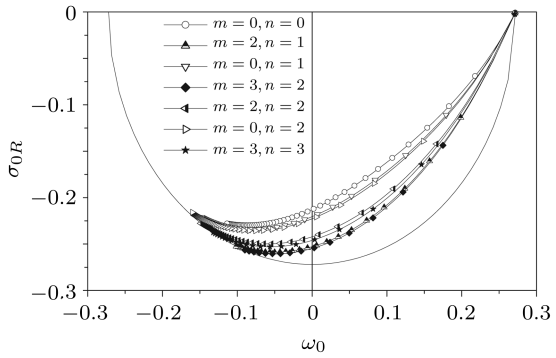


Fig.4. The distribution of the zeroth-order approximate eigenvalues, $\sigma_0 = \sigma_{0\mathrm{R}} - \mathrm{i}\omega_0$, on the complex σ_0 plane for various ε.

there is a unique neutral mode with $\sigma_R = 0$ for each of these acceptable (m,n) modes, corresponding to the critical number $\varepsilon_{*0}^{(m,n)}$. The most important conclusion can be drawn from these results is that the most dangerous global mode is the axi-symmetric mode $(0,0)$, which yields the largest critical number $\varepsilon_{*0}^{(0,0)} = 0.1590$.

Once the zeroth-order approximation of eigenvalue σ_0 is obtained, the first-order approximation of the eigenvalue σ_1 can be determined by using the formula (115) given in part (I).[1] Then, one can calculate the eigenvalue approximately by $\sigma \approx \sigma_0 + \varepsilon\sigma_1$.

The variations of the first-order approximation eigenvalues with ε for the case $\eta_0^2 = 0.01$ are shown in Figs.5, 6 and 7. The numerical results again show that the axi-symmetric mode $(0,0)$ is the most dangerous mode, which yields the largest critical number $\varepsilon_{*1}^{(0,0)}$ among all the acceptable global modes. The mode $(0,0)$, therefore, is selected, and determines the grand interfacial pattern at the late stage of dendritic growth.

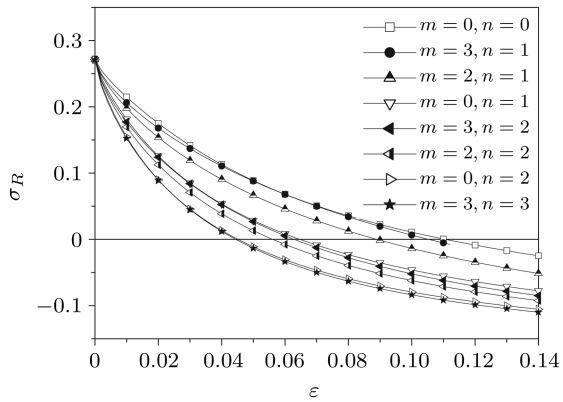


Fig.5. The variations of the real part of the first-order approximation of eigenvalues, σ_{R} with ε, of the modes $(0,0)$, $(0,1),(0,2)$; $(2,1),(2,2)$; $(3,2),(3,3)$ for the case $\eta_0^2 = 0.01$.

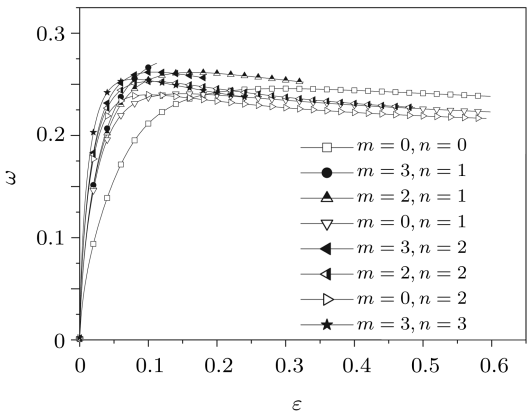


Fig.6. The variations of the imaginary part of the first-order approximation of eigenvalues, ω with ε, of the modes $(0,0)$,$(0,1)$,$(0,2)$; $(2,1),(2,2)$; $(3,2),(3,3)$ for the case $\eta_0^2 = 0.01$.

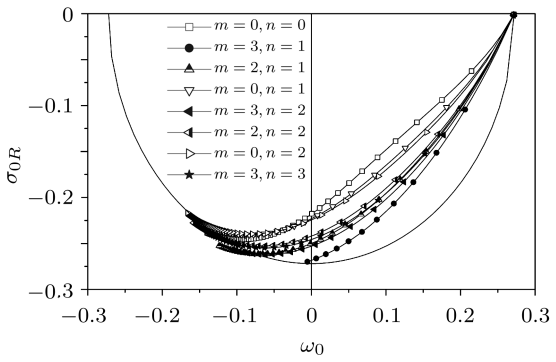


Fig.7. The distribution of the first-order approximation eigenvalues, $\sigma = \sigma_{\rm R} - {\rm i}\omega$, on the complex σ plane for various ε.

Note that in the zeroth-order approximation eigenvalue σ_0 is independent of the Peclet number η_0^2, while the eigenvalue σ in the first-order approximation, is a function of Peclet number. The numerical values of the critical numbers $\varepsilon_{*1}^{(m,n)}$ for the special case $\eta_0^2 = 0.01$ are given in Table 1. Our numerical results show that

$$\varepsilon_{*1}^{(0,0)} > \varepsilon_{*1}^{(3,1)} > \varepsilon_{*1}^{(2,1)} > \varepsilon_{*1}^{(0,1)} >$$

$$\varepsilon_{*1}^{(3,2)} > \varepsilon_{*1}^{(2,2)} > \varepsilon_{*1}^{(3,3)} > \varepsilon_{*1}^{(0,2)} > \cdots$$

The largest critical number is calculated to be $\varepsilon_{*1}^{(0,0)} = 0.1107$. It is deduced that the stability criterion is $\varepsilon_* = \varepsilon_*^{(0,0)} \approx \varepsilon_{*1}^{(0,0)}$; under this condition

$$\begin{cases} \text{as} \quad \varepsilon > \varepsilon_*, & \text{the system is globally stable;} \\ \text{as} \quad 0 < \varepsilon < \varepsilon_*, & \text{the system is unstable.} \end{cases}$$

More specifically, from Figs.2 and 5 one can conclude that when $\varepsilon_{*1}^{(0,1)} < \varepsilon < \varepsilon_{*1}^{(0,0)}$, the system has one axi-symmetric growing mode and infinitely many decaying modes; when $\varepsilon_{*1}^{(0,2)} < \varepsilon < \varepsilon_{*1}^{(0,1)}$, the system has two axi-symmetric growing modes and, in general, when $\varepsilon_{*1}^{(0,k)} < \varepsilon < \varepsilon_{*1}^{(0,k-1)}$, the system has k axi-symmetric growing modes. As $\varepsilon \to 0$, the eigenvalues of these growing modes apparently tend to the limit $\sigma_0 = (0.2722, 0.0)$.

Table 1. The critical numbers $\varepsilon_{*1}^{(m,n)}$ and the corresponding eigenvalues of the global neutral modes for the case of $\eta_0^2 = 0.01$.

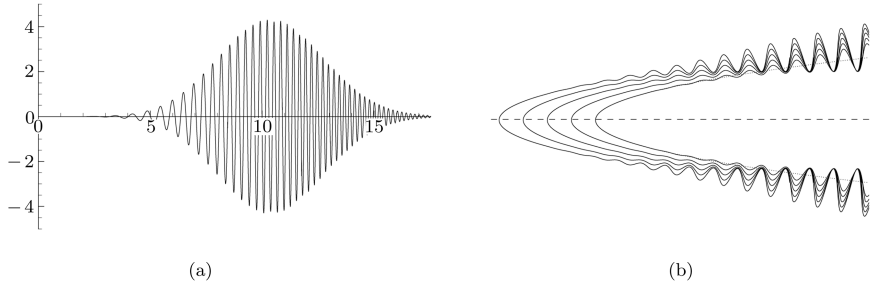
(m,n)	$\varepsilon_{*1}^{(m,n)}$	$\sigma = (\sigma_{\rm R} - {\rm i}\omega_*)$	ζ_c
$(0,0)$	0.1107	$(2\times10^{-6}, -0.2181)$	$(1.1547, -0.5074)$
$(0,1)$	6.4700×10^{-2}	$(1\times10^{-6}, -0.2231)$	$(1.3990, -0.4924)$
$(0,2)$	4.5153×10^{-2}	$(1\times10^{-6}, -0.2245)$	$(1.4787, -0.4835)$
$(2,1)$	8.8970×10^{-2}	$(1\times10^{-5}, -0.2500)$	$(1.4394, -0.2068)$
$(2,2)$	5.6130×10^{-2}	$(1\times10^{-6}, -0.2420)$	$(1.5220, -0.3008)$
$(3,2)$	6.2901×10^{-2}	$(1\times10^{-6}, -0.2530)$	$(1.5346, -0.1863)$
$(3,3)$	4.4457×10^{-2}	$(1\times10^{-6}, -0.2457)$	$(1.5717, -0.2647)$

The shape of dendritic interface corresponding to a global neutral mode can be written in the form:

$$\begin{aligned} &\eta_{\rm s}(\xi,\theta,t) \\ &\approx 1 + \varepsilon^2\eta_1(\xi,\theta) + \hat{h}_0(\xi){\rm e}^{-{\rm i}(\omega_* t/\eta_0^2\varepsilon_*)+{\rm i}m\theta} \\ &\quad (\text{as} \ \ \varepsilon \to 0), \end{aligned} \tag{57}$$

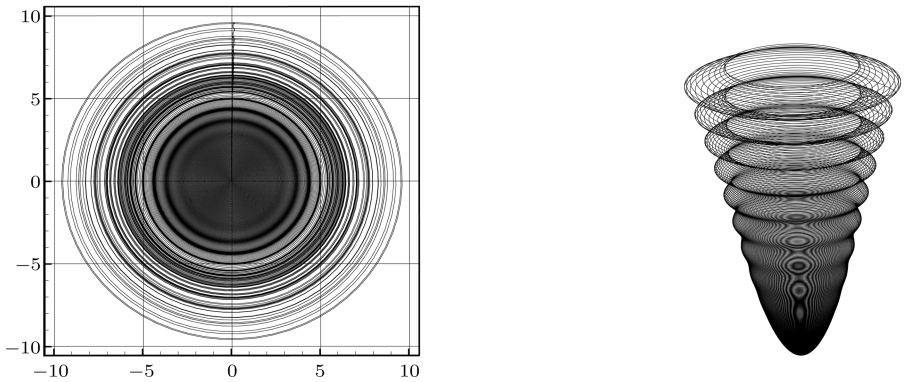
where $\eta_1(\xi,\theta)$ is the leading term in the regular perturbation expansion (RPE) part; while $\hat{h}_0(\xi){\rm e}^{-{\rm i}(\omega_* t/\eta_0^2\varepsilon_*)+{\rm i}m\theta}$ is the global neutral mode (m,n) in the SPE part. The parameter $\sigma = -{\rm i}\omega_*$ is the eigenvalue corresponding to the critical number $\varepsilon_* = \varepsilon_*^{(m,n)}$.

The shape of the eigen-function of the selected global neutral mode $(0,0)$ is shown in Fig.8. The interface shape of the selected global mode $(0,0)$ and its projection on the (x,y) plane are shown in Fig.9.



(a) (b)

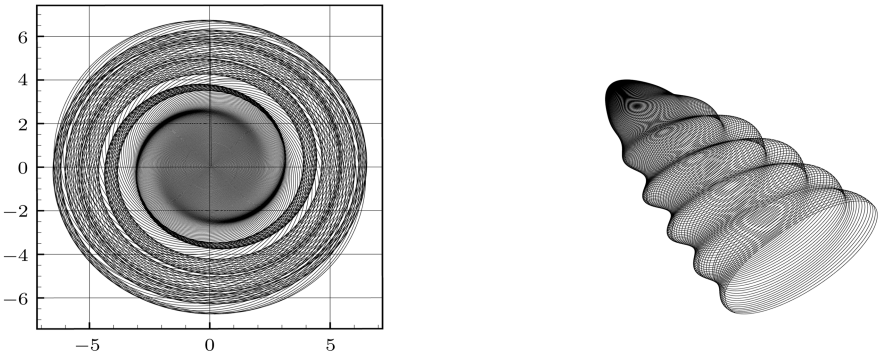
Fig.8. A typical GTW neutral mode: (a) the graphs of the eigenfunction; (b) the interface shapes in a time sequence.



(a) (b)

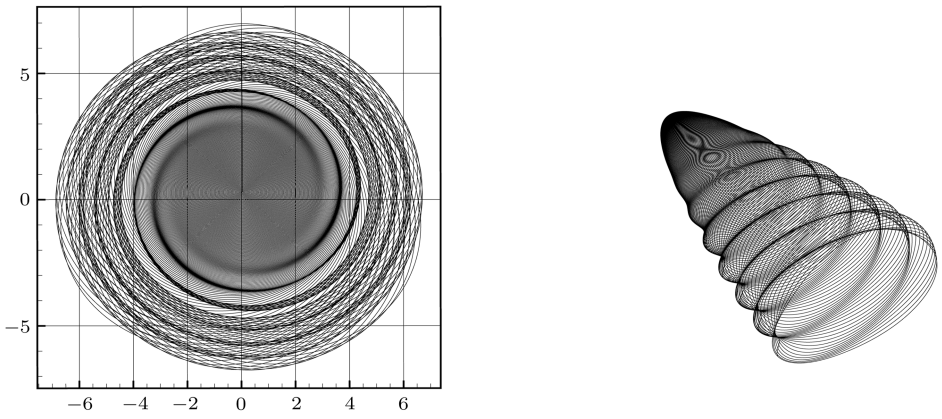
Fig.9. (a) The projection of the shape of interface global neutral mode (0,0) on (x, y)-plane; (b) The shape of interface of the selected global neutral mode (0,0).

The projections of the interface on the (x, y) plane and 3D graph of the interface shapes for the non-axisymmeric global neutral mode $(2, 1)$ and $(3, 2)$ are respectively shown in Figs.10 and 11, which describe the multi-arms spiral interfacial waves propagation along the Ivantsov's paraboloid. These spiral wave modes are decaying, as it was demonstrated before, when the selection condition $\varepsilon = \varepsilon_*^{(0,0)}$ was satisfied. The presence of the global spiral wave modes explored in this paper does not affect the stability mechanism and selection criterion $\varepsilon = \varepsilon_*^{(0,0)}$ derived by the IFW theory. Especially, the wave diagram for the axi-symmetric global wave modes as sketched in Fig.12 still remain.[3,4]



(a) (b)

Fig.10. The shape of interface of dendrite for the global neutral mode (2,1): (a) the projection of the interface on the (x, y) plane; (b) the 3D graph of the interface.



(a) (b)

Fig.11. The shape of interface of dendrite for the global neutral mode (3,2): (a) the projection of the interface on the (x, y) plane; (b) the 3D graph of the interface.

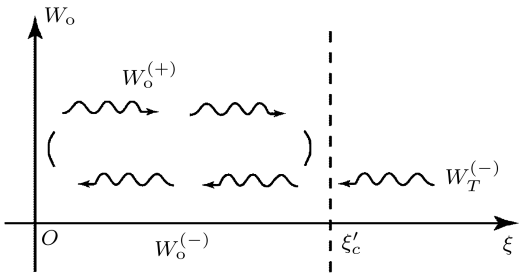


Fig.12. Wave diagram of the GTW mechanism.

Numerical computations show that in the regime of small undercooling, the critical number $\varepsilon_{*1}^{(m,n)}$ is approximately a constant. Especially, for the axisymmetric mode $(0,0)$ we have $\varepsilon_{*1}^{(0,0)} \approx 0.1107$. However, for large undercooling, say, $\mathrm{Pe}_0 > 1.0$, the situation is changed. The critical number $\varepsilon_{*1}^{(0,0)}$ decreases significantly as the undercooling temperature increases (see Fig.13).

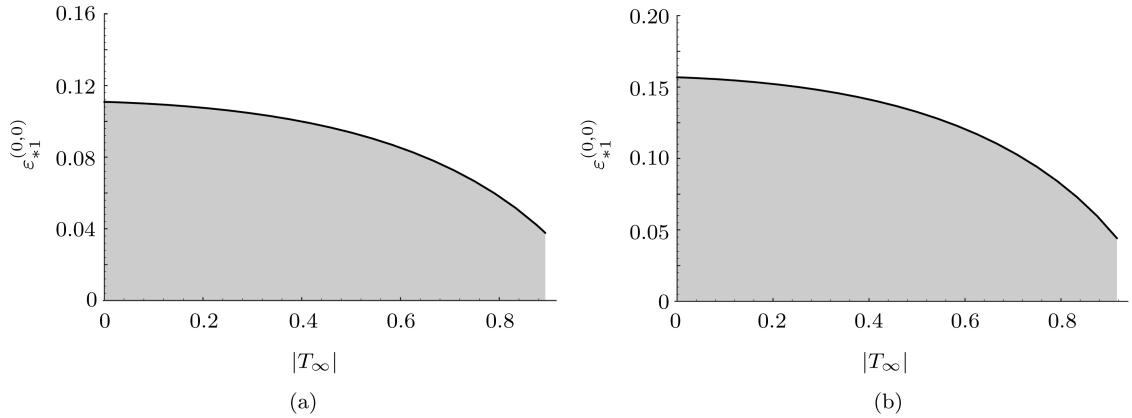


Fig.13. The variation of the critical number $\varepsilon_{*1}^{(0,0)}$ for the cases: (a) symmetric model; (b) one-sided model. The shaded region is the linearly unstable region of steady solutions.

With the selection criterion $\varepsilon = \varepsilon_*$ and using the capillary length ℓ_c as the length scale, the dimensionless tip velocity, dimensionless tip radius and frequency of oscillation can be uniquely determined by the given growth condition and material thermodynamic properties as follows:

$$U_\mathrm{tip} = \frac{U\ell_\mathrm{c}}{\kappa_\mathrm{T}} = \frac{\ell_\mathrm{c}}{\ell_\mathrm{T}} = \varepsilon_*^2\eta_0^2, \tag{58}$$

$$R_\mathrm{tip} = \frac{\ell_\mathrm{t}}{\ell_\mathrm{c}} = \frac{\ell_\mathrm{t}}{\ell_\mathrm{T}}\frac{\ell_\mathrm{T}}{\ell_\mathrm{c}} = \frac{\mathrm{Pe}}{\varepsilon_*^2\eta_0^4}, \tag{59}$$

$$\Omega_* = \frac{\omega_*}{\eta_0^2\varepsilon_*}. \tag{60}$$

The above theoretical predictions free of adjustable parameter are in excellent agreement with all available experimental data. Figure 14 shows the variation of tip velocity U_tip with undercooling temperature T_∞ and the comparison of the theoretical curve with experimental data; Figure 15 shows the variation of tip radius R_tip with undercooling temperature T_∞ and the comparison of the theoretical curve with experimental data. For more details, the reader can refer to Ref.[7].

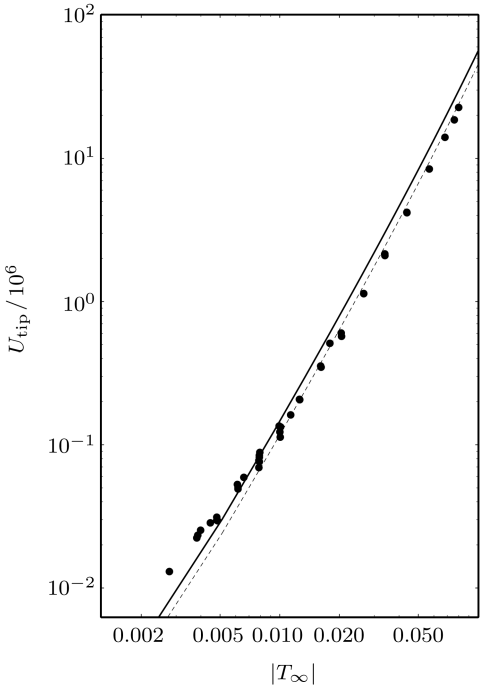


Fig.14. The variation of U_tip with $|T_\infty|$. The solid line is given by the IFW theory with zero anisotropy, $\alpha_4 = 0$. The dotted line is the modified IFW theory's results with the inclusion of the axial anisotropy of surface tension $\alpha_4 = 0.075$. The dots are the micro-gravity experimental data.

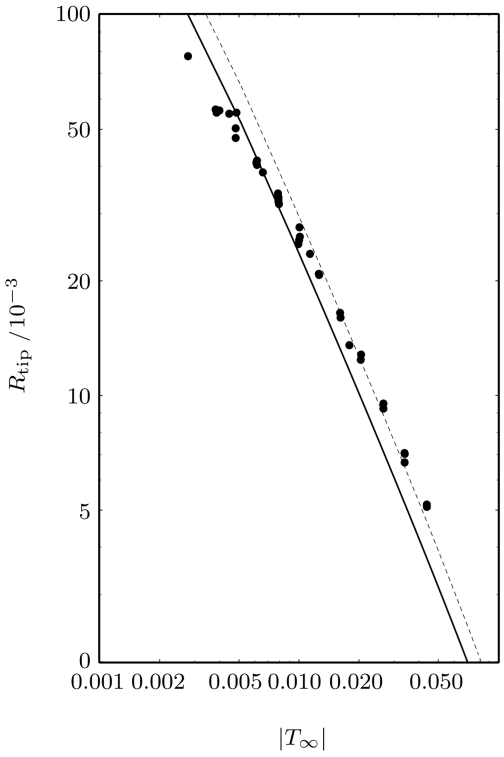


Fig.15. The variation of $R_{\rm tip}$ with T_∞. The solid line is given by the IFW theory with zero anisotropy, $\alpha_4 = 0$. The dotted line is the modified IFW theory's results with the inclusion of the axial anisotropy of surface tension $\alpha_4 = 0.075$. The dots are the micro-gravity experimental data.

It should be emphasized that there is a significant difference between the selection criterion ε_* given by the IFW theory and the selection criterion,

$$\sigma_* = \frac{2}{U_{\rm tip} R_{\rm tip}^2} \tag{61}$$

used by the MSC theory. The connection between these two parameters is

$$\sigma_* = 2\varepsilon_*^2 \left(\frac{\rm Pe_0}{\rm Pe}\right)^2 . \tag{62}$$

The parameter $\rm Pe_0 = \eta_0^2$ is just a function of T_∞, while Pe may be affected by all physical parameters involved in the system, such as surface tension, anisotropy, flow effects, etc. It is found that only for the case of small undercooling and small anisotropy of surface tension, $\rm Pe \approx Pe_0$, so that, as an approximation one has $\sigma_* \approx 2\varepsilon_*^2$. However, when the parameter of anisotropy of surface tension α_4 is large, the ratio $\left(\frac{\rm Pe_0}{\rm Pe}\right)$ may be quite large (refer to Refs.[8], [9] and [10]. Therefore, it is not surprising, that there is the case for dendritic growth, in which the ε_*-criterion may be significantly different from the σ_*-criterion.

6. Conclusions

Based on the investigations carried out in the present work, the following main conclusions can be drawn:

(i) In addition to a discrete set of axi-symmetrical global wave modes corresponding to the infinite number of index $n = 0, 1, 2, \ldots$ that has been found by the original IFW theory, it is confirmed that the system also allows some non-axi-symmetrical global wave modes.

(ii) The physically acceptable unstable non-axi-symmetrical global modes of dendritic growth are identified to be $(2,1)$, $(2,2)$, $(3,2)$, $(3,3)$, etc., which describe the multiple-arms spiral waves propagating along the Ivantsov's paraboloid.

(iii) However, these unstable spiral waves are less dangerous, compared with the axi-symmetric mode $(m = n = 0)$, explored previously in the IFW theory. As a consequence, the global stability criterion and selection condition $\varepsilon = \varepsilon_* = \varepsilon_*^{(0,0)}$ discovered originally by the IFW theory remains valid.

(iv) The selection criterion ε_* is significant different from the selection criterion σ_* historically proposed by the MSC theory. The numerical value of ε_* varies significantly with the undercooling temperature, especially in the high undercooling regime. The relation between these two criterion parameters, $\sigma_* = 2\varepsilon_*^2 \left(\frac{\rm Pe_0}{\rm Pe}\right)^2$ contains the factor $\left(\frac{\rm Pe_0}{\rm Pe}\right)$, which is not always negligible and may be a factor much larger than one. For instance, dendritic growth with large anisotropic surface tension may be just the case.

References

[1] Chen Y Q, Tang X X and Xu J J 2009 *Chin. Phys.* B **18** 671

[2] Xu J J 1989 *Phys. Rev.* A **40** 1599

[3] Xu J J 1991 *Phys. Rev.* A **43** 930

[4] Xu J J 1997 *Interfacial Wave Theory of Pattern Forma-*

tion: Selection of Dendrite Growth and Viscous Fingering in a Hele–Shaw Flow (New York: Springer) p27–180
[5] Bender C M and Orszag S A 1978 *Advanced Mathematical Methods for Scientists and Engineers* (New York: McGraw–Hill) p107–136
[6] Abramovitz M and Stegun I A 1964 *Handbook of Mathematical Functions* (National Bureau of Standards) p360
[7] Xu J J and Yu D S 2001 *J. Crystal Growth* **222** 399
[8] Chen X J, Chen Y Q, Xu J P and Xu J J 2008 *Front. Phys. China* **3** 418
[9] Xu J P 2008 *The Effects of Anisotropic Surface Tension and Interface Kinetics on 3-D Steady Needle Growth* (Master Degree Thesis, Nankai University, Tianjin, China, May, 2008) p44, p45
[10] Chen X J 2008 *Gibbs–Thomson Condition and Steady Needle Growtrh with Anisotropic Surface Tension* (Master Degree Thesis, Nankai University, Tianjin, China, May, 2008) p42